Received: 4 May 2016 | Revised: 1 November 2016 | Accepted: 26 November 2016

DOI: 10.1002/tal.1354

WILEY

SPECIAL ISSUE PAPER

Pseudodynamic tests with substructuring of a full-scale precast box-modularized structure made of reinforced concrete shear walls

Guoshan Xu[1,2] | Zhen Wang[1,2] | Bin Wu[1,2] | Oreste S. Bursi[3] | Xiaojing Tan[4] | Qingbo Yang[5] | Long Wen[1,2] | Hongbin Jiang[1,2]

[1] Key Lab of Structures Dynamic Behavior and Control of the Ministry of Education, Harbin Institute of Technology, Harbin, China

[2] School of Civil Engineering, Harbin Institute of Technology, Harbin, China

[3] Department of Civil, Environment & Mechanical Engineering, University of Trento-Italy, Trento, Italy

[4] Yunnan Institute of Building Research, Kunming, China

[5] Jiangsu Power Design Institute Co., Ltd. of China Energy Engineering Group, Nanjing, China

Correspondence
Guoshan Xu, School of Civil Engineering, Harbin Institute of Technology, Harbin 150090, China.
Email: xuguoshan@hit.edu.cn

Funding information
The National Key Research and Development Program of China, Grant/Award Number: 2016YFC0701106; The National Science Foundation of China, Grant/Award Number: 51161120360, 51308159 and 51408157; A Set of Technology Study and Engineering Application Examples for Building Industrialization in Yunnan Province, Grant/Award Number: 2012CA025

Summary

A novel horizontal and vertical wall-to-wall and wall-to-floor connection methods for precast box-modularized structure with reinforced concrete shear walls (PBSRCSWs) are proposed in this paper. The entailing behavior of the proposed connections and the seismic performance of one full-scale six-story PBSRCSWs were experimentally studied by means of pseudodynamic substructure tests. In order to improve the relevant experimental accuracy, we presented and validated one versatile testing platform Hytest, combined with external displacement feedback control (EDFC; Hytest with EDFC). In greater detail, it was shown from the pseudodynamic substructure test results that the proposed Hytest with EDFC can effectively impose the desired displacements on the specimens rather than on the actuators. Moreover, both the horizontal and vertical wall-to-wall connections proposed for the PBSRCSWs exhibited a favorable behavior whilst the PBSRCSWs subjected to earthquake records showed an excellent seismic performance.

KEYWORDS

concrete connection, external displacement feedback control, precast box-modularized structure, pseudodynamic substructure test, reinforced concrete shear wall, seismic performance

1 | INTRODUCTION

1.1 | Background and motivation

The precast concrete construction can provide high-quality production with minimal construction time and represents an effective way to promote industrialization; therefore, it has been of great interest around the world in recent decades. A single standardized three-dimensional precast component was used as the repetitive modular construction element. This unit was then combined together to form different house types. The structure—Habitat '67—was composed of clusters of house units one on top of the other.[1] Previous research on seismic precast structures goes back to the Precast Seismic Structural Systems Research Program in the early 1990s.[2] Since then, a significant amount of research has been conducted worldwide on the design and seismic behavior of precast concrete frame structures and precast concrete shear wall structures. The research on precast concrete shear wall structures was mostly focused on the connections of different types, that is, emulative,[3–5] posttensioned,[6,7] hybrid,[8,9] and in posttensioned walls endowed with energy dissipation.[10,11]

In order to enhance the earthquake resistance of emulative precast concrete walls, Kang et al.[4] proposed that bonded or unbonded longitudinal rebars with a partially reduced cross-sectional area can be used at the plastic hinge zone. Henin and Morcous[3] investigated the use of nonproprietary bar splice sleeves for precast concrete construction, and the test results indicated that the proposed bar splice sleeves exhibit adequate capacity to fully develop reinforcing bars while being simpler to use and more economical than current

proprietary splice sleeves. An assembly method was then proposed for precast reinforced concrete shear walls using dry connection through a horizontal steel connector (H-connector) and high-strength bolts.[5] In addition, one design-oriented analytical model to estimate the nonlinear lateral load behavior of unbonded posttensioned walls was introduced and validated with available experimental results.[7] The effects of tendon layout, tendon end-anchorage configuration, and external vertical load on the self-centering ability of unbonded posttensioned precast concrete shear walls subjected to earthquake loading were investigated by Erkmen and Schultz.[6] Conversely, Smith et al.[8] presented the behavior of a hybrid precast concrete wall specimen, which was characterized by a combination of mild steel and high-strength unbonded posttensioning steel for lateral resistance across horizontal joints. Along the same line, the lateral load behavior comparison of hybrid precast concrete shear wall test specimens with a precast specimen designed to emulate monolithic cast-in-place

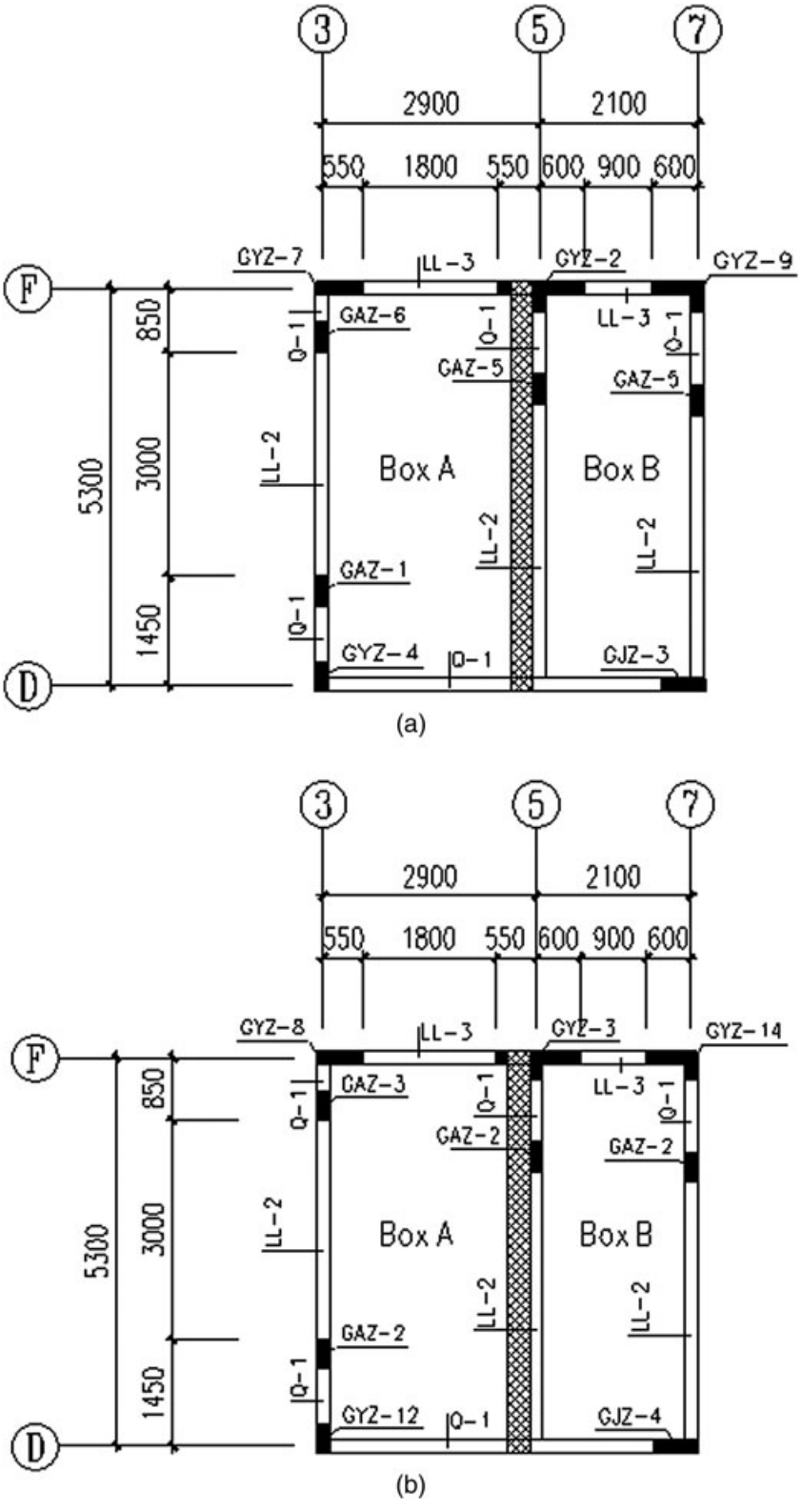

FIGURE 1 Plan view of the precast box-modularized structure with reinforced concrete shear walls: (a) first story; (b) other stories

reinforced concrete (RC) shear walls was conducted by Smith et al.,[9] and the results showed the potential for the use of precast walls in seismic regions. Moreover, the results of three half-scale self-centering precast concrete jointed walls incorporating energy dissipators were described by Restrepo and Rahman.[10] Finally, an innovative precast concrete wall system consisting of a precast wall with end columns was introduced by Sritharan et al.[11]; they combined a precast unbonded posttensioned wall with two end columns using a set of special cost-effective energy-dissipating connectors.

The aforementioned investigations on precast shear wall structures were normally conducted using quasi-static testing; however, due to the predetermined displacement protocol, the corresponding experimental results cannot directly disclose the seismic performance of an overall structure subjected to the earthquake randomness. Conversely, the pseudodynamic testing (PDT) or pseudodynamic substructure testing (PDST) method can economically and accurately trace the seismic response of a structure with a large or even full-scale structure model.[12] In fact since it was proposed in the late 1960s, the PDT has been systematically investigated worldwide, and the research has mostly focused on improving the experimental accuracy operating on integration algorithms, actuator control, model updating, finite element software, and testing platform.

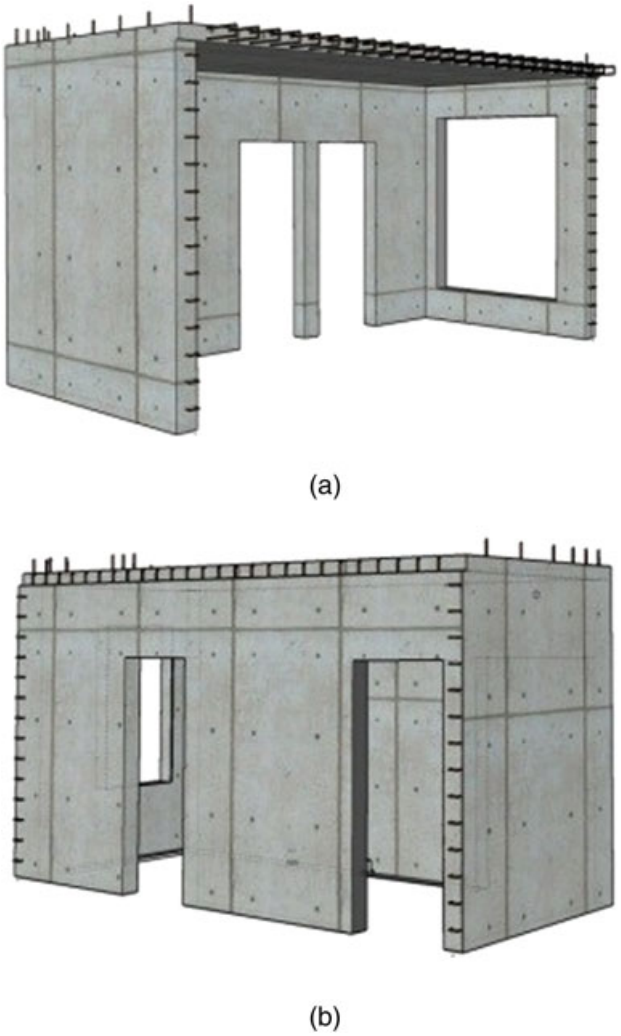

FIGURE 2 Model of Boxes A and B in each story: (a) Box A; (b) Box B

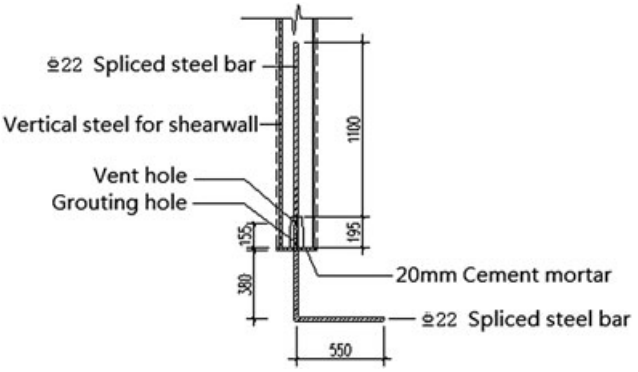

FIGURE 3 Details of horizontal wall-to-wall connection

The integration algorithm is the key element of the PDT, PDST, and real-time substructure testing (RST), which is a new testing methodology. There are several new variants that have been investigated and applied in recent years.[13–20] The operator-splitting method for RST and the equivalent force control method for PDT and RST were investigated by Wu et al.[20] and Chen et al.[17] Chang[15] presented the improved explicit Chang method for structural dynamics and Bursi et al.[14] investigated novel coupling Rosenbrock-based algorithms for real-time dynamic substructure testing. Bonnet et al.[13] presented a comparison of methods for the analysis of the numerical substructure in a real-time hybrid test, and a multitasking strategy was described capable of satisfying the various control and numerical requirements. Chen et al.[16] proposed an unconditionally

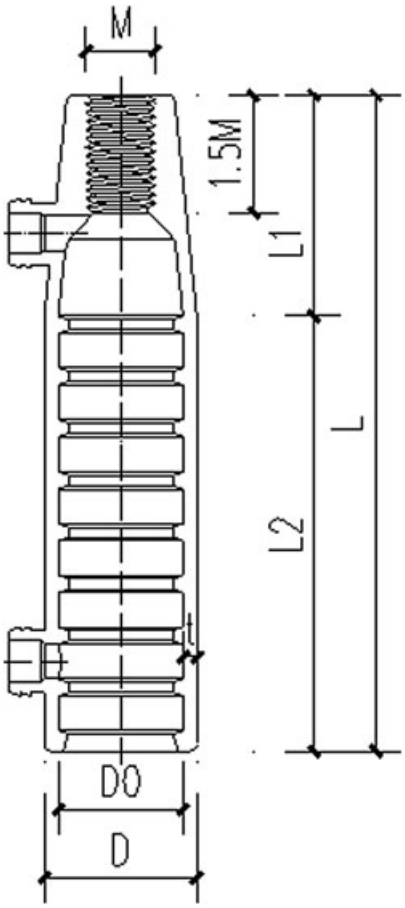

FIGURE 4 Details of the sleeve

TABLE 1 Dimensions of the sleeve (mm)

Type	L	L1	L2	D	M	D0	t
GTB4-22-A	195	69	126	48	23	38	5

stable explicit CR integration algorithm for real-time hybrid testing. Both, the actuator control and the corresponding delay compensation represent key elements of the RST, and there are several new types of methods that have been proposed; see, among others, Wang et al.,[21] Chae et al.,[22] Dong et al.,[23] and Ou et al.[24]

With regard to the use of FE software, a peer-to-peer Internet online hybrid test system incorporating OpenSEES and ABAQUS was developed by Wang et al.,[25] and the applicability of the proposed approach was numerically verified with a simple steel moment-resisting frame. With reference to online model updating for substructure pseudodynamic hybrid simulation, Kwon and Kammula[26] improved the PDST experimental accuracy by applying calibrated weighting factors at each time step to the relevant numerical models. The model updating with a constrained unscented Kalman filter for hybrid testing was investigated by Wu and Wang.[27] Moreover, the hybrid simulation of a multispan RC viaduct with plain bars and sliding bearings was conducted by Abbiati et al.[28] with an offline updating. One software framework for distributed experimental computational simulation of structural systems—OpenFresco—was proposed by Takahashi and Fenves[29] and a framework for multi-site simulation and application to complex structural systems-UI-Simcor was proposed and validated by Kwon et al.[30] Nonetheless, one platform capable of achieving an accurate control on the deformations of the specimens instead of the actuator displacements is yet to be set.

1.2 | Scope

Although much progress has been made on the research of precast concrete shear wall structures, new types of joint connections and the corresponding seismic performance of overall structure are still need to be investigated. Because the basic assembly elements of precast concrete shear wall structures are normally chosen to be individual shear wall, one faces time-consuming and complicated assemblies of elements and corresponding constructions of post-cast regions. In this respect, new types of assembly elements with easy construction connections are desirable. Furthermore, for accurately disclosing the seismic performance of newly proposed structures,

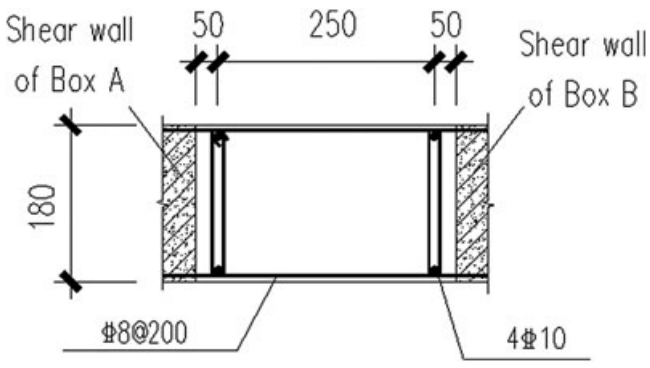

FIGURE 5 Details of vertical wall-to-wall connection

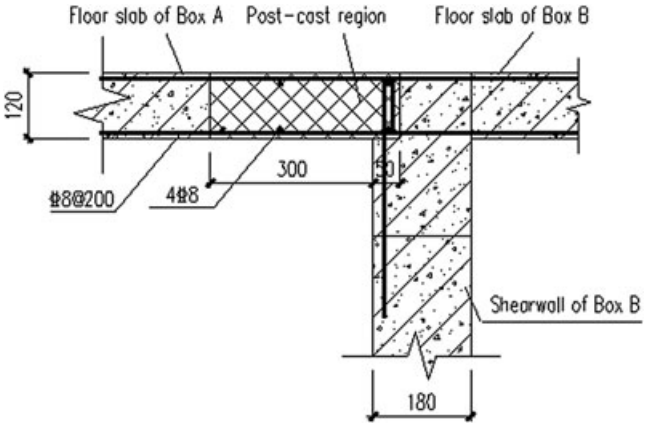

FIGURE 6 Details of the wall-to-floor slab connection

one versatile PDST platform, which can realize an accurate deformation control of the specimen, is still necessary to be developed.

In order for us to contribute to the solution of the aforementioned problems, this paper proposes, in Section 2, a novel precast box-modularized structure with reinforced concrete shear walls (PBSRCSWs) and the corresponding wall-to-wall and wall-to-floor connections. Section 3 introduces both the specimen and the test setup, whereas Section 4 presents and validates a high-accuracy PDST platform combined with external displacement feedback, that is,

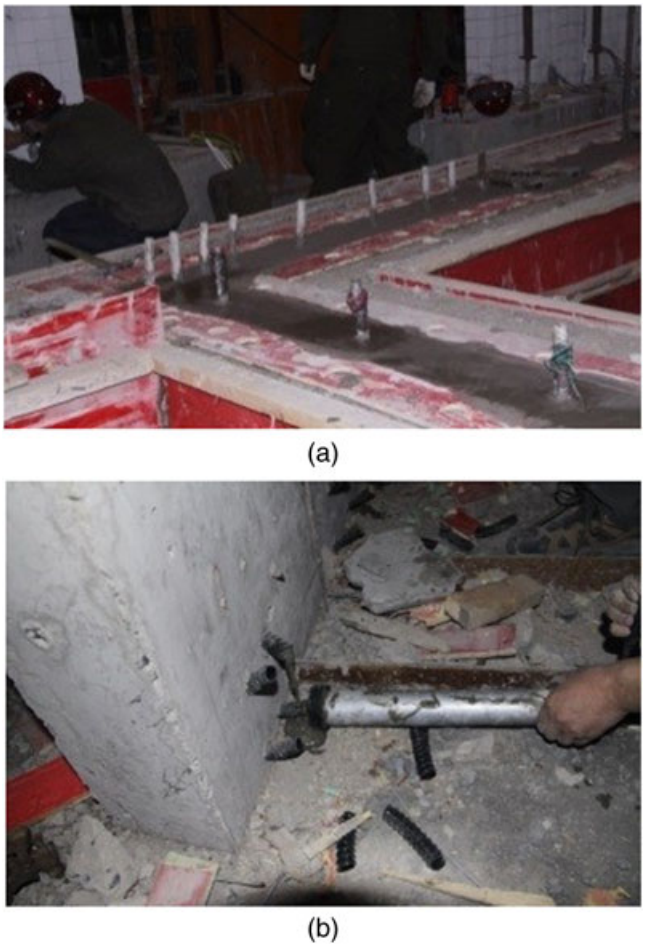

FIGURE 7 Pictures of the horizontal wall-to-wall connection: (a) steel bars for connecting upper story walls; (b) grouting of the sleeve

HyTest with external displacement feedback control (EDFC). Both the responses of the proposed connections and the relevant seismic performances traced with the HyTest platform are discussed in Section 5. Finally, conclusions are summarized in Section 6.

2 | DESIGN OF THE PRECAST BOX-MODULARIZED STRUCTURE

2.1 | Building configuration

The design motivation of PBSRCSWs is the program named "A Set of Technology Study and Engineering Application Examples for Building Industrialization in Yunnan Province." The program aims to build and popularize the PBSRCSWs affordable building in Yunnan Province. The prototype structure was designed according to the China Code for Seismic Design of Buildings, and the corresponding design requirement of peak ground acceleration (PGA) is 400 gal (= 4 m/s^2). The representative building configuration of the PBSRCSWs is shown in Figure 1.

Instead of individual shear wall, the box module was selected as the basic assembling element in PBSRCSWs, in order to provide high-quality and easy installation production with minimal construction time. The Boxes A and B in Figure 1 are depicted in Figure 2 for each story. The building has an interstory height of 3,000 mm and plan dimensions of 5,300 × 2,900 mm for Box A and 5,300 × 2,100 mm for Box B. The thicknesses of the wall and floor are 180 and 120 mm, respectively. A concrete class C30 is used for the precast walls and floors, C40 for the post-cast regions, and C60 for the grouting materials. The longitudinal steel bars for the shear wall are S10@250, and the horizontal ones for the shear wall and floor slab are S8@200. The longitudinal steel bars for elements GAZ and GYZ are S12, S14, S16. The stirrups for GAZ and GYZ are S8 and S10. For convenience of the transformation and installation of Boxes A and B, parts of the wall are infilled with lightweight polystyrene boards, such as the wall under coupling beam LL-2, and this type of wall is called infilled wall throughout this paper.

FIGURE 8 Picture of the vertical wall-to-wall connection

FIGURE 9 Picture of the whole connections

2.2 | Design of connections

The reliability of the connection between shear walls greatly affects the structural integrity and seismic behavior, and hence, it is the key element for the PBSRCSWs. Three types of joint connections should be considered in the PBSRCSWs, that is, the horizontal wall-to-wall connection, vertical wall-to-wall connection, and the horizontal wall-to-floor connection. With the aim to improve both structural integrity and seismic behavior, we propose and use three types of new connection methods together for the PBSRCSWs in this paper: (a) a horizontal wall-to-wall connection characterized by vertical reinforcements spliced indirectly by single-row grout-filled sleeves; (b) a vertical wall-to-wall connection characterized by a stirrup bolted with vertical reinforcements; (c) a horizontal non-composite wall-to-floor slab connection.

TABLE 2 Properties of the concrete

Element	Story	Class of concrete	Number of samples	Average compressive strength/MPa	Cube compressive strength/MPa
Wall and floor slab	First	C30	3	36.7	34.8
Wall and floor slab	Second	C30	3	39.4	37.4
Post-cast concrete	First	C40	3	47.6	45.2
Post-cast concrete	Second	C40	3	44.8	42.6
Grouting material	Both	C60	3	74.1	70.4

2.2.1 | Horizontal wall-to-wall connection

With the aim to both design and develop engineering applications for affordable houses, this paper utilizes a connection technology characterized by "vertical reinforcements spliced indirectly by one single-row of steel bars centrally grouted in a sleeve in horizontal joint connections" for PBSRCSWs, as shown in Figure 3. The connection technology is named as "single-row grout-filled sleeve connection" throughout this paper. The details and the dimensions of the sleeve are shown in Figure 4 and Table 1. The quantity and diameter of the steel bars for the vertical reinforcements indirectly spliced can be determined by the principle that the area of the steel bars is equal to the area of the spliced reinforcements in the wall. In this paper, 91 S22 spliced steel bars are used for the two-story shear wall horizontal connection. The length of the steel bar is determined in such a way that it meets the requirements of the Chinese Code for Design of Concrete Structures. The steel bars for connecting the lower story wall are screwed into the sleeves before anchoring them at the predetermined position at the bottom central line of the wall. The corrugated pipes are then installed on both the grouting hole and the vent hole of the sleeves. The steel bars for connecting the upper story wall are anchored at the predetermined position on the top central line of the wall with a sleeve connection length of 145 mm outside of the wall. The concrete was cast after all the connecting steel bars, sleeves, and reinforcements for Boxes A and B were shaped. The sleeves were fully grouted by a self-leveling grouting material after the upper stories of Boxes A and B are assembled, as shown in Figure 3.

2.2.2 | Vertical wall-to-wall connection

Figure 5 shows the details of the vertical connection of wall-to-wall characterized with a stirrup bolted by vertical reinforcement. There is a 350 mm wall-to-wall post-cast region and 50 mm aligned U-shaped reinforcements outside of the walls on Boxes A and B. The construction of the post-cast region starts with the placement of 4S10 vertical steel bars and a series of S8 horizontal stirrups. The template is fixed, and then the concrete is cast.

TABLE 3 Properties of the steel bars

Type and grade	Symbol	d/mm	f_y/MPa	f_u/MPa
HRB400	S	8	410.3	651.9
HRB400	S	10	427.4	673.1
HRB400	S	12	458.6	611.5
HRB400	S	14	468.2	624.3
HRB400	S	16	455.9	607.8
HRB400	S	22	467.5	618.2

2.2.3 | Horizontal wall-to-floor connection

Figure 6 presents the details of the horizontal connection of wall-to-floor characterized by a non-composite floor slab joint connection. When Boxes A and B are assembled, there is a 350 mm post-cast region of floor slab to floor slab, a series of 330 mm U-shaped reinforcements outside of the Box A floor slab, a series of 330 mm bottom reinforcements outside of the Box B floor slab, and a series of L-shaped reinforcements starting from the top of the Box B floor slab and anchored to the wall of Box B. The construction of the post-cast region starts with the placement of 4S8 steel bars. The template is fixed, and then the concrete is cast.

3 | EXPERIMENTAL SPECIMEN AND SETUP

3.1 | Overview of the specimen

In view of the capabilities of the loading facilities at the Structural and Seismic Testing Center of the Harbin Institute of Technology, one six-story structure—with the plan view shown in Figure 1—was chosen. It was estimated that the nonlinear behavior of the investigated six-story structure was mainly concentrated on the bottom of the structure. Therefore, the experiments were carried out using PDST, with the bottom two stories as the experimental substructure and the upper four stories as the numerical substructure.

Because the weight of each box is approximately 270 kN, special lifting tools and equipment are necessary to assemble the boxes, although this is not the focus of this paper. For convenience, Boxes A and B in the first story are manufactured separately at the experimental site in the laboratory, and Boxes A and B in the second story are manufactured on the first story 2 weeks later than the pouring of the concrete for the first story. To simulate the effect of the box assembling, we use cement mortar for leveling and separating the two stories. Figure 7 shows both the shear wall horizontal connections and the grouting of the sleeves. In addition, Figures 8 and 9 depict the shear wall vertical connection and the whole connections, respectively.

3.2 | Material properties

Material tests were performed to obtain basic mechanical properties of the materials. Compression and tensile tests were carried out using a universal testing machine at the Structural and Seismic Testing Center, Harbin Institute of Technology. From each concrete batch, three 100 mm edged cube samples were taken. The cube compressive strength of concrete is obtained by multiplying 0.95 by the measured average compressive strength according to the Chinese Standard for

(a)

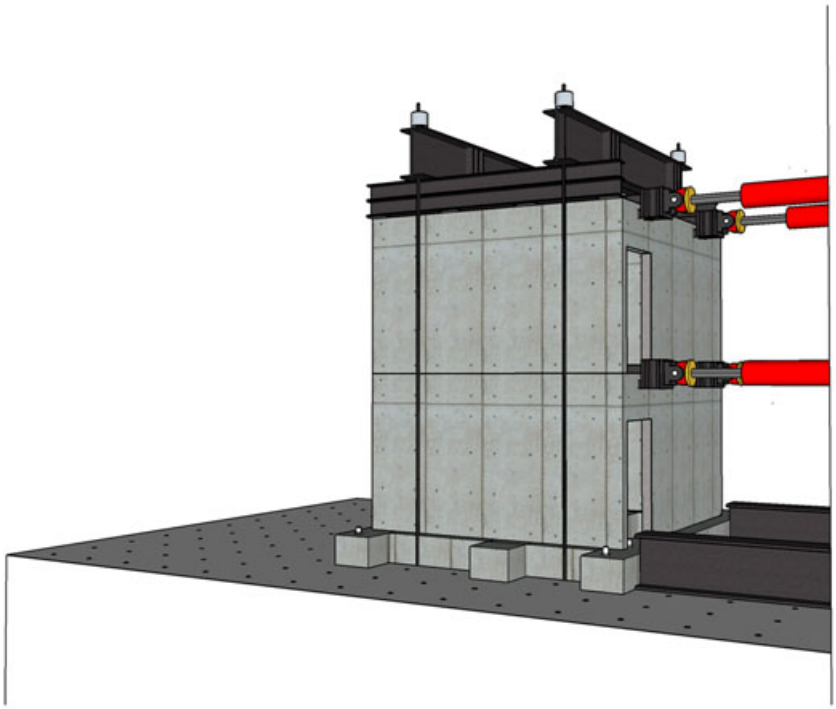

(b)

FIGURE 10 Test setup: (a) picture of the test setup; (b) 3-D model of the test setup

Test Method of Mechanical Properties on Ordinary Concrete. The results of the compression tests obtained on the cubic samples are presented in Table 2. Samples of steel bars of each diameter were collected and tested. The experimentally obtained properties are presented in Table 3. A more resistant concrete for the post-cast joints was utilized in this paper in order to promote the integrity and seismic behavior of the PBSRCSWs. Although a more resistant concrete for the post-cast joints may induce more stresses in the joints, a minor difference in resistant was a compromise to be accepted. The performance of the post-cast regions are necessary to be evaluated by PDSTs.

3.3 | Test setup

The test setup is comprised of a two-story PBSRCSWs specimen, reaction wall, four servo-hydraulic actuators, eight steel connection beams, four vertical steel reaction frames, posttensioned steel bars, and

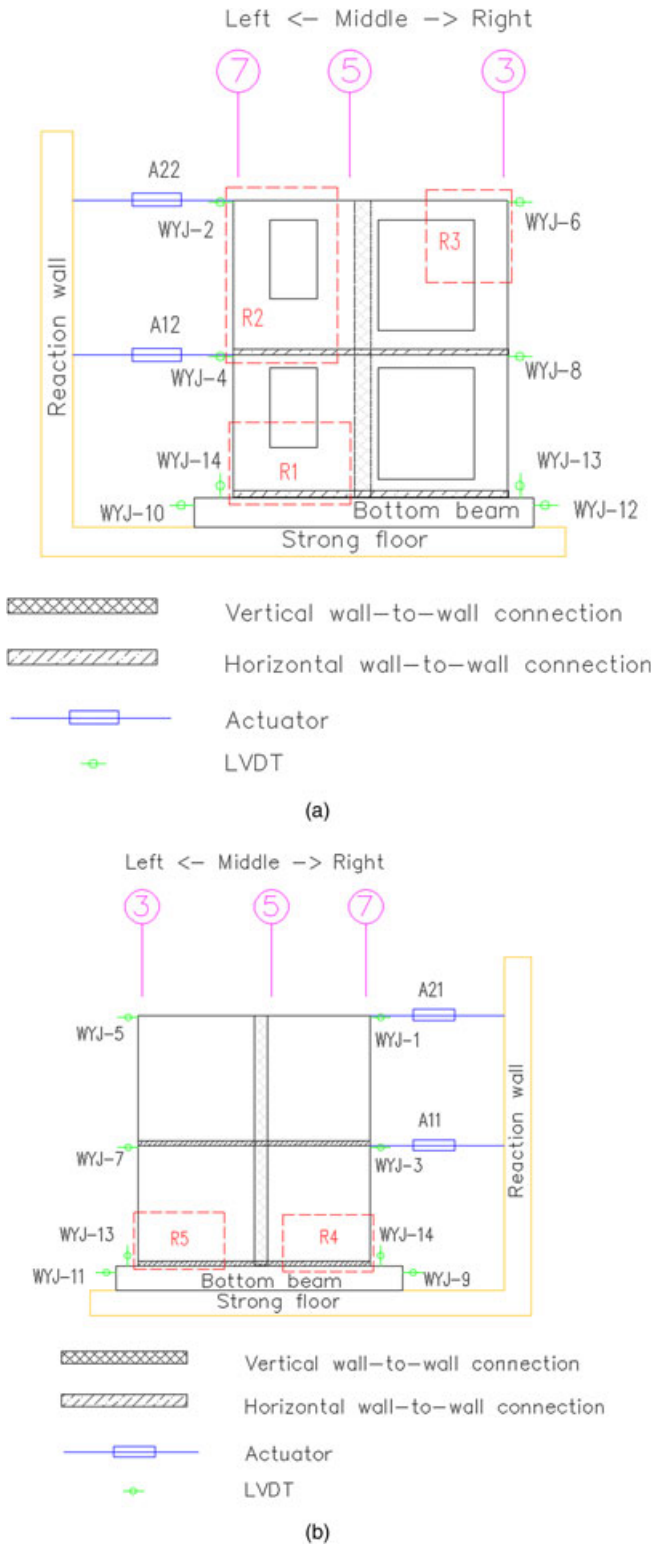

FIGURE 11 Layout of transducers and actuators: (a) front view of Line F; (b) front view of Line D. LVDT = linear variable displacement transducer

anchor bolts. A general view of the test setup and the layout of transducers and actuators are presented in Figures 10 and 11, respectively. Two MTS servo-hydraulic actuators named A21 and A22, with a stroke of ±250 mm and a loading capacity of ±1,000 kN, were used on the second floor. Two MTS actuators numbered A11 and A12, with a stroke of ±250 mm and loading capacities of ±1,000 and ±2,000 kN, respectively, were used on the first floor. The loading of each actuator acted at the central line of the floor slab on each story. Each actuator was connected to the specimen through two steel connection beams that were bolted on the top and bottom of the floor slab. In order to take into account the weight of the upper stories, we adopt 20 posttensioned steel bars and attachments, as shown in Figure 10. In this way, the P-Δ effect is not accounted for during the tests. However, it is shown by numerical analyses that the influence of the P-Δ effect was negligible.

The deformation of the specimen was monitored by 14 linear variable displacement transducers (LVDTs, named from WYJ-1 to WYJ-14), as presented in Figure 11. The transducers numbered from WYJ-1 to WYJ-4 are fixed around to the actuators along Line 7, and the transducers numbered from WYJ-5 to WYJ-8 are fixed at the corresponding position along Line 3. For monitoring the eventual slippage of the bottom beam, transducers numbered WYJ-9 and WYJ-10 are fixed along Line 7, and transducers numbered WYJ-11 and WYJ-12 are fixed along Line 3. The measured deformations on the specimen corresponding to each actuator can be calculated by that the average value of two LVDTs corresponding to the actuator minors the average value of two relevant LVDTs on the bottom beam, that is, $d11 = \frac{WYJ\text{-}3+WYJ\text{-}7}{2} - \frac{WYJ\text{-}9+WYJ\text{-}11}{2}$, $d12 = \frac{WYJ\text{-}4+WYJ\text{-}8}{2} - \frac{WYJ\text{-}10+WYJ\text{-}12}{2}$, $d21 = \frac{WYJ\text{-}1+WYJ\text{-}5}{2} - \frac{WYJ\text{-}9+WYJ\text{-}11}{2}$, $d22 = \frac{WYJ\text{-}2+WYJ\text{-}6}{2} - \frac{WYJ\text{-}10+WYJ\text{-}12}{2}$, in which d11 and d12 are specimen deformations corresponding to actuators A11 and A12 in the first story, respectively, and d21 and d22 are specimen deformations corresponding to actuators A21 and A22 in the second story, respectively. For monitoring the vertical displacements of the bottom beam, transducers numbered WYJ-13 and WYJ-14 are used. In PDSTs, the damage on the specimen was observed, especially the regions marked by dash lines in Figure 11—named from R1 to R5—were mostly concerned and will be described in Subsection 5.1.

3.4 | Implementation of the PDST

A six degrees of freedom (6DoF) lumped mass model of the investigated PBSRCSWs was used in the PDSTs, with the bottom two DoFs as the experimental substructure and the upper four DoFs as the numerical substructure. The corresponding mass, stiffness, and damping matrix are so determined that the simulation results with the lumped mass model are similar to the simulation results provided by OpenSEES finite element model. The lumped mass of each story was calculated to be 4.591×10^4 kg. The interstory stiffness of the numerical substructure for the 3rd, 4th, 5th, and 6th stories were chosen to be 463.4, 352.2, 255, 144.7 kN/mm, respectively, and they remained unchanged during the PDSTs. The damping of the structure was determined such that the damping ratio was 5% for both the first and second mode of vibration. The El Centro (NS, 1940) earthquake record with PGAs of 70, 125, 220, 400, and 620 gal was tested by the HyTest. The Central Difference method with a time interval of 0.01 s was chosen as time integration algorithm. It is shown from simulation result comparisons between the 6DoFs lumped model and OpenSEES finite element model that the response of the simplified model is nearly identical to the response of the finite element model. The results indicate that the simplified 6DoFs lumped mass

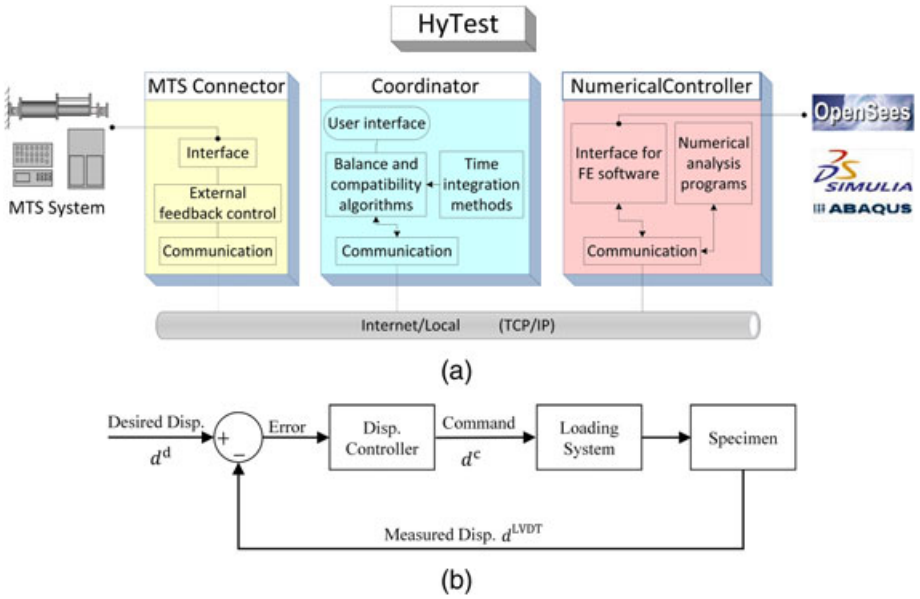

FIGURE 12 Framework of the HyTest with external displacement feedback control: (a) main components of HyTest; (b) block diagram of the external displacement feedback control. LVDT, linear variable displacement transducer; TCP, transmission control protocol; IP, internet protocol

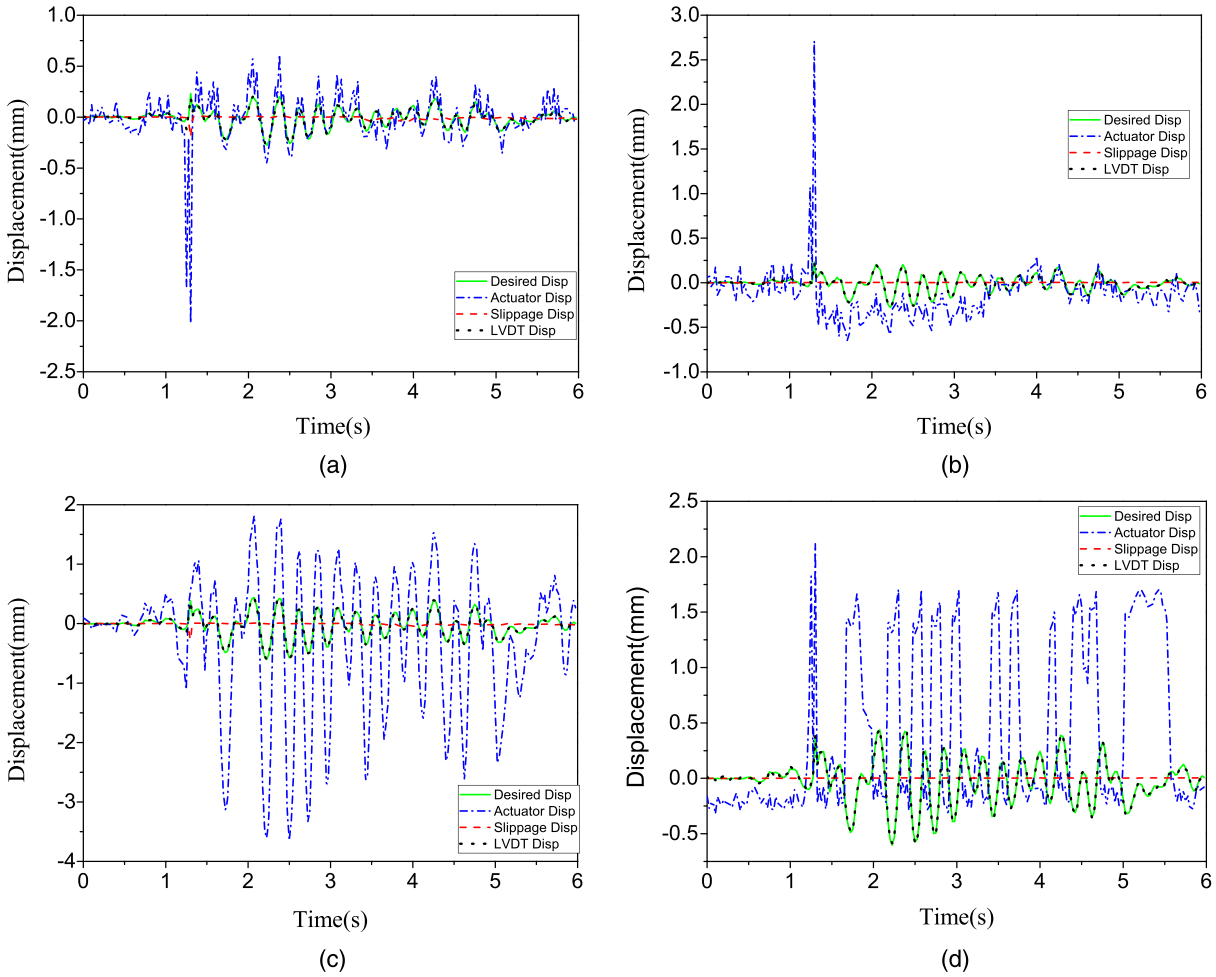

FIGURE 13 Displacement time histories for a pseudodynamic substructure testing of 70 gal peak ground acceleration: (a) histories related to Actuator A11; (b) histories related to Actuator A12; (c) histories related to Actuator A21; (d) histories related to Actuator A22. LVDT = linear variable displacement transducer

TABLE 4 Mean values of displacement differences for a PDST with 70 gal PGA

Item	A11 (mm)	A12 (mm)	A21 (mm)	A22 (mm)
|Desired Disp-LVDT Disp|	0.01	0.02	0.01	0.01
|Desired Disp-Actuator Disp|	0.2	0.3	1	0.5

Note. LVDT = linear variable displacement transducer; PDST = pseudodynamic substructure testing; PGA = peak ground acceleration.

TABLE 5 Mean values of displacement differences for a PDST with 400 gal PGA

Item	A11 (mm)	A12 (mm)	A21 (mm)	A22 (mm)
|Desired Disp-LVDT Disp|	0.5	1.5	3.0	1.0

Note. LVDT = linear variable displacement transducer; PDST = pseudodynamic substructure testing; PGA = peak ground acceleration.

model is an alternative for the PDSTs. Therefore, in the PDSTs, the horizontal deformations were simulated by high-accuracy servo-hydraulic actuators, the weight of the upper four stories were simulated by posttensioned steel bars, and the overturning moment on the boundary was neglected. It should be mentioned that the PDSTs for PGAs of 70, 125, and 220 gal were conducted by HyTest combined with EDFC (HyTest with EDFC), but not the large PGAs of 400 and 620 gal. One reason is that the influence of the limited joint gaps and the deformation of supports and connectors was comparably small for large deformations of the structure when subjected to large earthquakes. Another reason was for safety considerations. If the LVDT failed to properly measure the deformations of the specimen, in case of the specimen suffers serious local damage or even collapse under large earthquake, the PDSTs may fall out of control. Therefore, the EDFC is highly recommended for the PDSTs of small earthquakes.

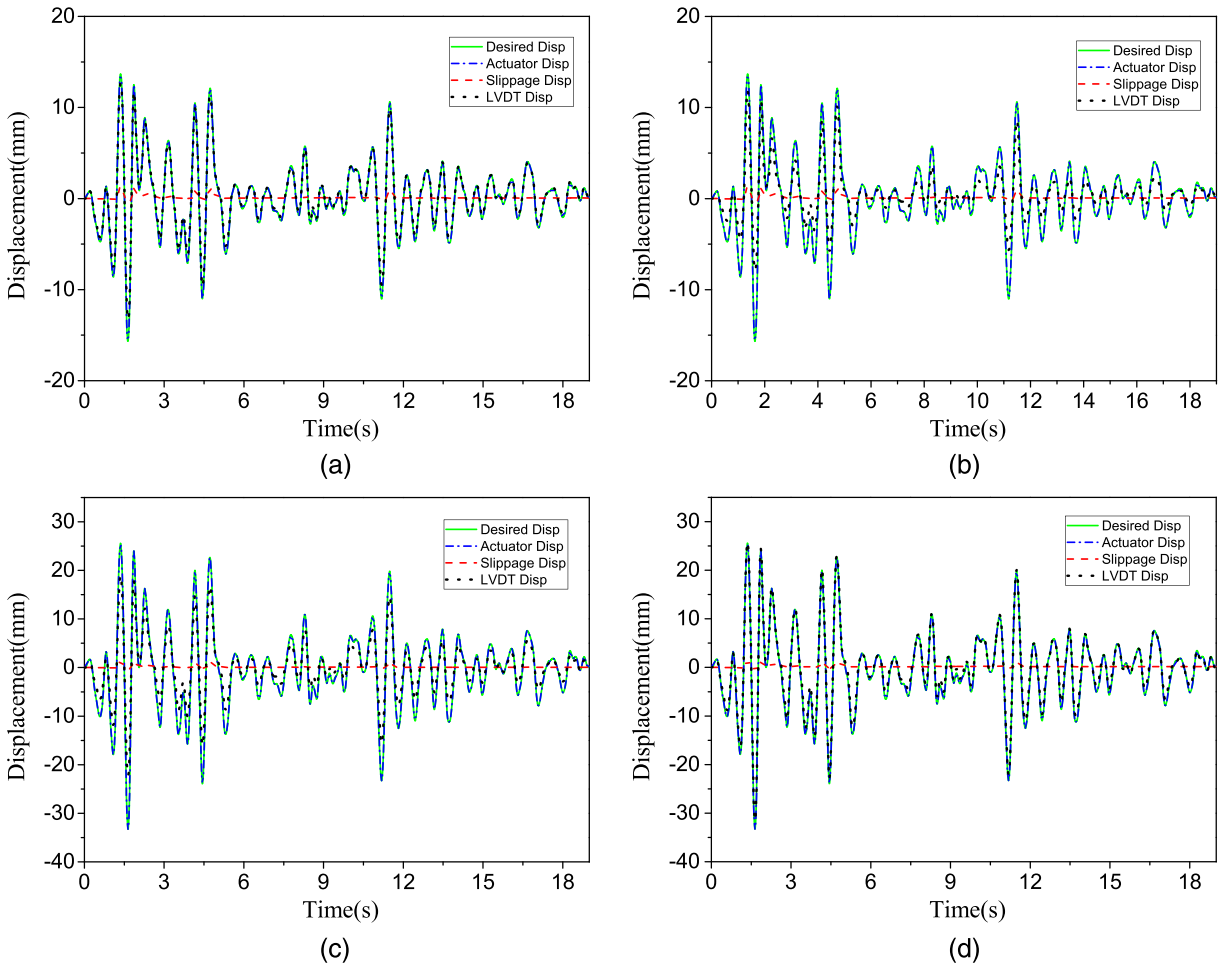

FIGURE 14 Displacement time histories for a pseudodynamic substructure testing with 400 gal peak ground acceleration: (a) histories related to Actuator A11; (b) histories related to Actuator A12; (c) histories related to Actuator A21; (d) histories related to Actuator A22. LVDT = linear variable displacement transducer

4 | THE HyTesT PLATFORM WITH EDFC

4.1 | The framework of the HyTest with external displacement feedback control

In order for us to carry out a more accurate investigation with hybrid testing, a new platform called HyTest is under development at the Harbin Institute of Technology. As shown in Figure 12a, this testing platform consists of three main components, namely, MTS Connector, Coordinator, and Numerical Controller. The Coordinator module is designed to solve the equations of motion of the emulated structure using an explicit or implicit time integration algorithm. The Numerical Controller is to communicate with finite element software, including OpenSEES and Abaqus, whereas the Connector is used to communicate with MTS system. The internet or intranet using socket communication protocol is available for communicating data between components. When utilizing this platform, the emulated structure should be split into a dynamic part and one or more static parts. The dynamic part is evaluated within the coordinate, while the static parts can be physically tested or numerically simulated. If necessary, some static parts are numerically simulated using finite element software. In this way, this platform can perform different kinds of hybrid simulation, or even distributed hybrid simulation. The objective of this platform is not only to investigate the hybrid testing methodology but also to implement hybrid testing to evaluate structural seismic performance. Therefore, this software is written using the commonly used Visual C++ and provides friendly client interface. Furthermore, compared with other available hybrid testing platforms, such as OpenFresco[29] and UI-Simcor,[30] the HyTest can realize accurate control on the deformations of specimens instead of the displacements of actuators by the EDFC strategy.

Joint gaps and elastic or even elastic–plastic deformation of supports and connectors for actuators are inevitable in PDT or PDST, especially for specimens with comparably large stiffness, as in this paper. Meanwhile, non-negligible slippage often occurs between the specimen bottom beam and the laboratory strong floor. Research reveals that these loading errors can accumulate and propagate in the test. For accurately disclosing the seismic performance of structures with reliable testing results, especially for PDT or PDST with a relatively weak earthquake, where the structural responses are small, effective measures or even an effective feedback control method must be taken. Even it is not a new topic in the field of PDT or hybrid testing, this is critical for a platform of hybrid testing. In addition, it is a good choice to implement control algorithm on a common PC. As far as the authors' knowledge, this platform is the first one that successfully performs outer loop control for hybrid testing on PC using a sampling interval less than settling time of the testing system.

The EDFC method shown in Figure 12b is adopted in HyTest to eliminate the loading errors aforementioned in the PDSTs. The measured actual deformations d^{LVDT} of the specimen are measured with 12 high-accuracy LVDTs and fed back to compare with the corresponding desired displacements d^{desired}, which are the calculated displacements provided by the time integration algorithm. The errors e between the measured and desired displacements are then converted

FIGURE 15 Failure modes of the infilled wall at R1 on Line F: (a) pictures at 220 gal peak ground acceleration (PGA); (b) pictures at 400 gal PGA; (c) pictures at 620 gal PGA

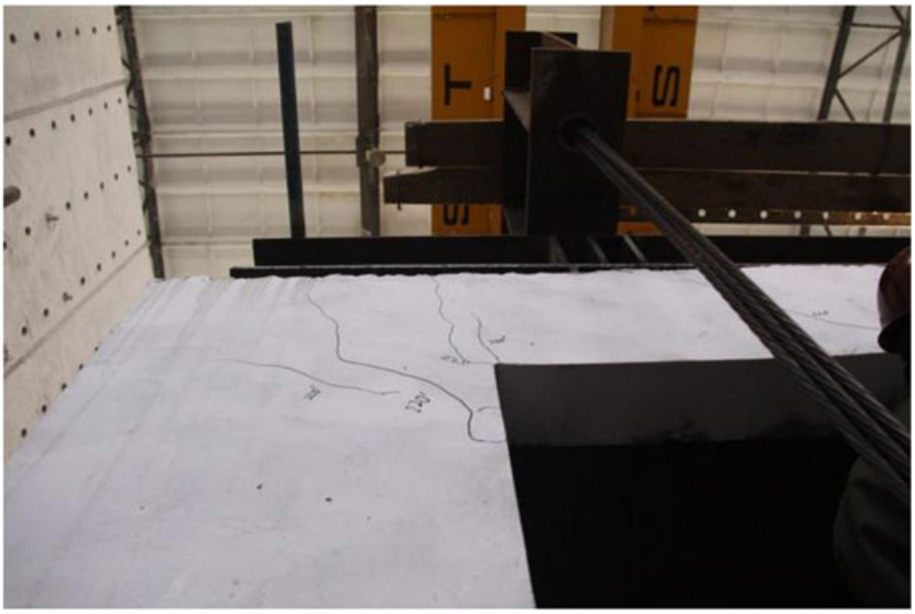

(a)

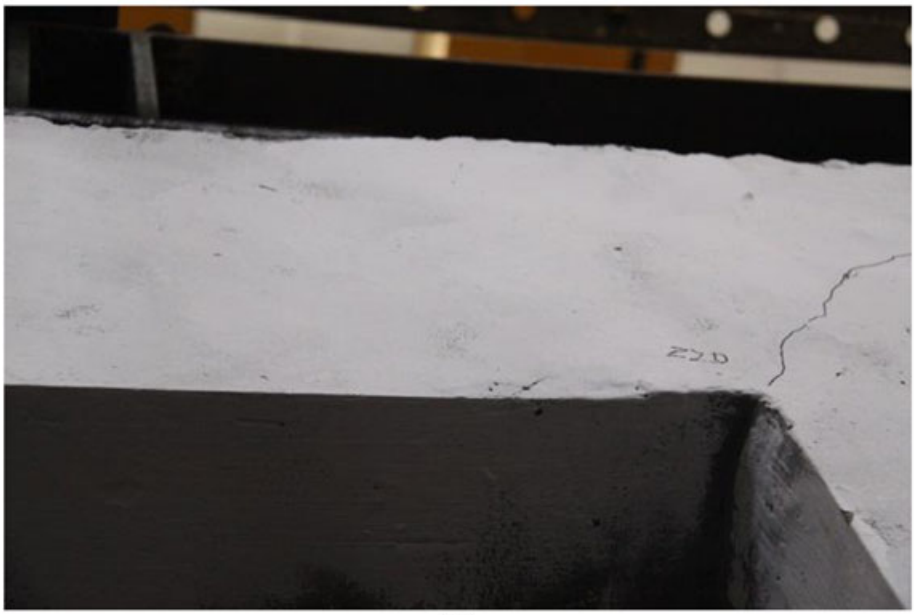

(b)

FIGURE 16 Failure mode of the coupling beam on Line F corresponding to 220 gal peak ground acceleration: (a) R2 on Line F; (b) R3 on Line F

to actuator commands d^{cmd} by a displacement controller, such as a proportional–integral (PI) controller. As well known, the proportional–integral controller can be expressed in the time domain as

$$d_{j,k+1}^{\mathrm{cmd}} = K_{\mathrm{P}} \cdot \left(d_j^{\mathrm{desired}} - d_{j,k}^{\mathrm{LVDT}} \right) + K_{\mathrm{I}} \cdot \int_0^t \left(d_j^{\mathrm{desired}} - d_{j,k}^{\mathrm{LVDT}} \right) dt, \tag{1}$$

in which K_{P} and K_{I} are proportional and integral gains, respectively. Using the following quadrature formula the integral reads

$$d_{j,k+1}^{\mathrm{cmd}} = K_{\mathrm{P}} \cdot \left(d_j^{\mathrm{desired}} - d_{j,k}^{\mathrm{LVDT}} \right) + \sum_{p=0}^{k} K_{\mathrm{I}} \cdot \left(d_j^{\mathrm{desired}} - d_{j,p}^{\mathrm{LVDT}} \right) \cdot \Delta \mathrm{t}, \tag{2}$$

which is the expression used in the tests.

Running the EDFC on a common PC is promising, because this can communicate with testing control software using digital signal instead of the complicated and costly real-time digital signal-processing board. However, it is a challenge due to the uncertainty of communication delay between HyTest and MTS system. For resolving this problem, the maximum communication delay was measured to be 35 ms, and the sampling interval in PDSTs was set greater than this maximum delay value, namely, 100 ms. However, one should know that this interval is much smaller than the settling time of the loading system. Online tuning of proportional and integral gains was performed before PDSTs as well. In view of the possible change of the communication delay during tests, the delay is online monitored and warning information is given when the communication delay is larger than the predetermined sampling interval. Fortunately, no warning information was found for the PDSTs in this paper, and it shows the effectiveness of the control method.

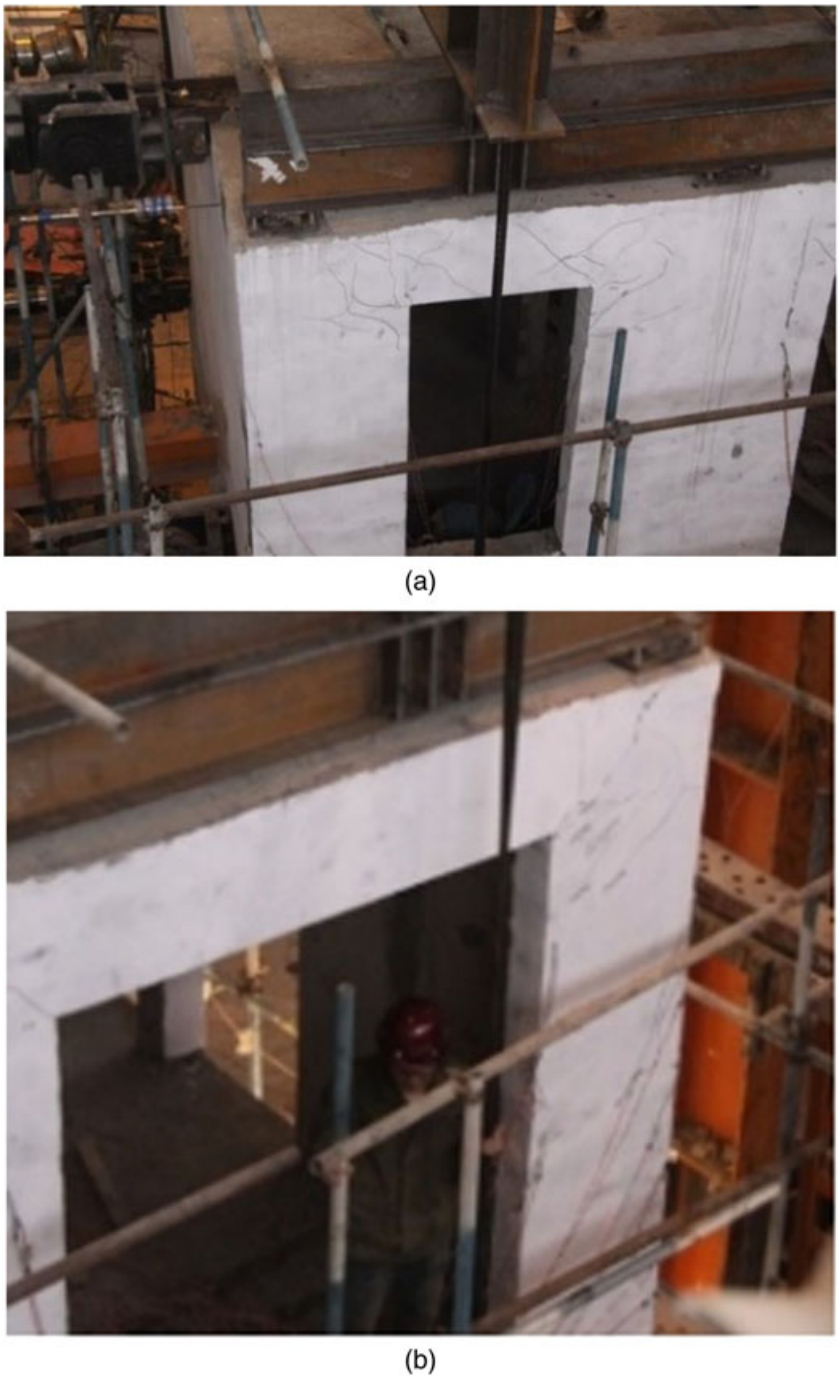

FIGURE 17 Failure mode of the coupling beam on Line F for 400 gal peak ground acceleration: (a) R2 on Line F; (b) R3 on Line F

4.2 | Experimental validation of the HyTests with EDFC

4.2.1 | Main results with EDFC

PDST with the El Centro (NS, 1940) Earthquake record with a PGA of 70 gal was performed to validate the effectiveness of the EDFC method. Figure 13 shows the displacement time histories related to four actuators. In this figure, "Desired Disp" denotes the target displacement of each story, computed by the Central Difference method, whereas "Slippage Disp" means the average of two LVDTs at the bottom beam—such as WYJ-9 and WYJ-11 or WYJ-10 and WYJ-12—to monitor the movement of the bottom beam. "LVDT Disp" means the measured deformations of specimen corresponding to each actuator by external LVDTs. "Actuator Disp" means the actuator displacements measured by the displacement transducers internal to the actuator. It is clearly shown from Figure 13 that the LVDT displacements almost overlap with the desired displacements for all actuators, while a great difference can be observed for the actuator displacement. This indicates that the joint gaps and/or deformation of the supports and connectors are effectively compensated. On the other hand, for the case of PDSTs without the EDFC, the actuator displacements should be close to the desired displacements, whereas the actual deformations of the specimen measured by LVDTs must be different from the desired ones. Therefore, the displacement control errors will induce errors in the measured restoring forces and distort the test results. To demonstrate the improvement with the EDFC method quantitatively, we analyze the displacement differences. Taking Actuator A21, for example, the maximum difference between the desired

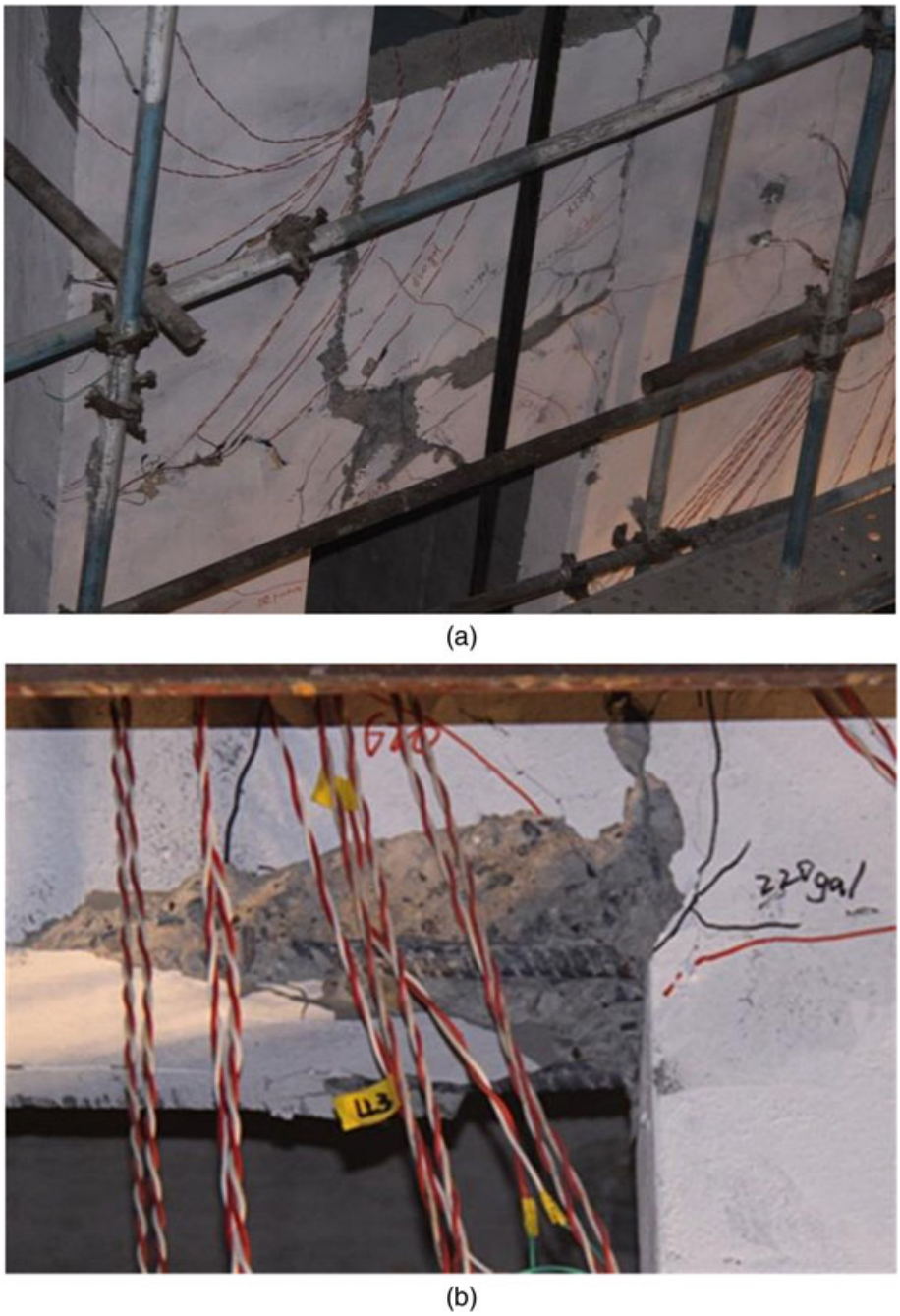

FIGURE 18 Failure mode of the coupling beam on Line F for 620 gal peak ground acceleration: (a) R2 on Line F; (b) R3 on Line F

displacement and the actuator displacement is approximately 3 mm, while that between the desired displacement and the LVDT just approximately 0.02 mm. The mean values of the displacement differences are given in Table 4. The maximum mean value of the difference between the desired displacement and the actuator displacement is approximately 1 mm, while that between the desired displacement and the LVDT is only approximately 0.02 mm. Meanwhile, the differences between two measured deformations at the same story, such as d11 and d12 for the first story or d21 and d22 for the second story, are so small that the structure moves as a stiff body and rotation is negligible. A sharp displacement difference can be observed approximately 1.2 s in Figure 13, such as A11. The reason is that the LVDT measurement system is disturbed. For us to save space, similar results of PDSTs with PGAs of 125 and 220 gal are not presented herein.

4.2.2 | Main results without EDFC

The PDST results for a 400 gal PGA without EDFC are reported in Table 5 and Figure 14. The differences between the desired displacements and the actuator displacements are negligible in the case of PDSTs without EDFC. It is clearly shown in Figure 14 that the actuator displacements almost overlap with the desired displacements for all actuators, while a big difference can be observed for the LVDT displacements. The maximum mean value of the difference between the desired displacement and the actuator displacement is negligible, while that between the desired displacement and the measured LVDT displacement is approximately 3.0 mm. The error maybe induced by the gaps and elastic–plastic deformations of connectors for actuators and the slippage between the specimen

(a)

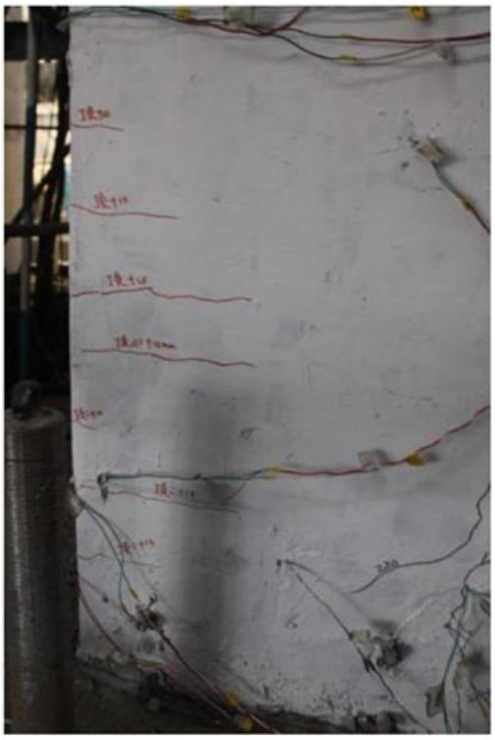

(b)

FIGURE 19 Failure mode of the wall limb on first story for 220 gal peak ground acceleration: (a) R4 on Line D; (b) R1 on Line F

bottom beam and the laboratory strong floor. The influence of the error was relatively small for large deformations of the structure when subjected to large earthquakes (such as in Figure 14, the error is about 3.0 mm, while the peak value of the response is about 30 mm) compared to small deformations of the structure when subjected to small earthquakes (such as in Figure 13, the error is about 1 mm, while the peak value of the response is just about 0.5 mm). It should also be noted that the test results may be influenced by control errors, but in view of test safety, this was an acceptable compromise. Similar results can be obtained from the PDST with a PGA of 620 gal. The comparisons with the results related to PGAs of 70, 125, and 220 gal indicate the effectiveness of the proposed HyTest endowed with the EDFC method. The proposed Hytest with EDFC method is highly recommended for PDSTs, especially for small earthquakes.

5 | EXPERIMENTAL RESULTS

5.1 | Test observations

The failure modes of the six-story PBMSRCSWs were observed for each PDST. In a greater detail, the measured displacements of

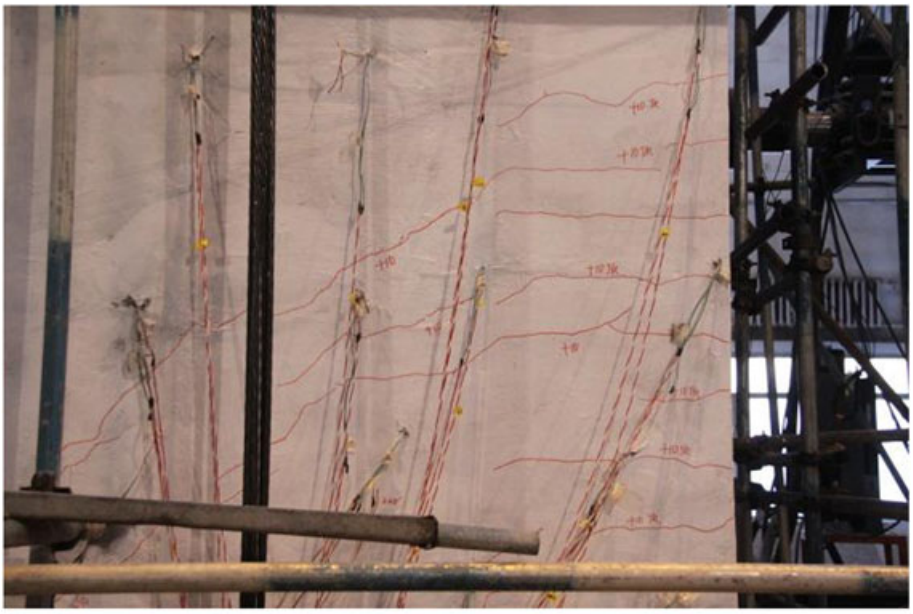

(a)

(b)

FIGURE 20 Failure mode of the wall limb on first story for 400 gal peak ground acceleration: (a) R4 on Line D; (b) right corner of R4 on Line D

WYJ-13 and WYJ-14 were negligible. Moreover, there were no visible failures on the proposed vertical and horizontal connections of wall-to-wall and wall-to-floor joints; conversely, both damages and failures were concentrated on the infilled walls, the coupling beams, and the wall limbs. The cracks and failure modes of the infilled walls, the coupling beams, and the wall limbs in PDSTs will be introduced hereafter, in which the marked Regions R1 to R5 can be located in Figure 11.

5.1.1 | Failure modes of the infilled walls

There were no visible damage on the infilled walls when the structure was subjected to the El Centro (NS, 1940) earthquake record with PGAs of 70 and 125 gal, and the corresponding maximum interstory drift was 0.68 mm. Figure 15 presents the failure modes of the infilled walls at Region R1 on Line F from PDSTs with PGAs of 220, 400, and 620 gal. The first series of cracks on the infilled wall occurred vertically at the boundary of the shear wall and infilled wall and horizontally under the openings when the specimen was subjected to a 220 gal PGA, and the corresponding maximum interstory drift was 8.9 mm. When subjected to a PGA of 400 gal, the corresponding maximum interstory drift was 17.6 mm, the previous cracks constantly expanded and extended, and the corresponding concrete cover was slightly damaged. The damage to the infilled wall can be easily repaired. When subjected to a PGA of 620 gal, the corresponding maximum interstory drift was 27.5 mm, the previous cracks widened, and the spalling of the cover concrete occurred.

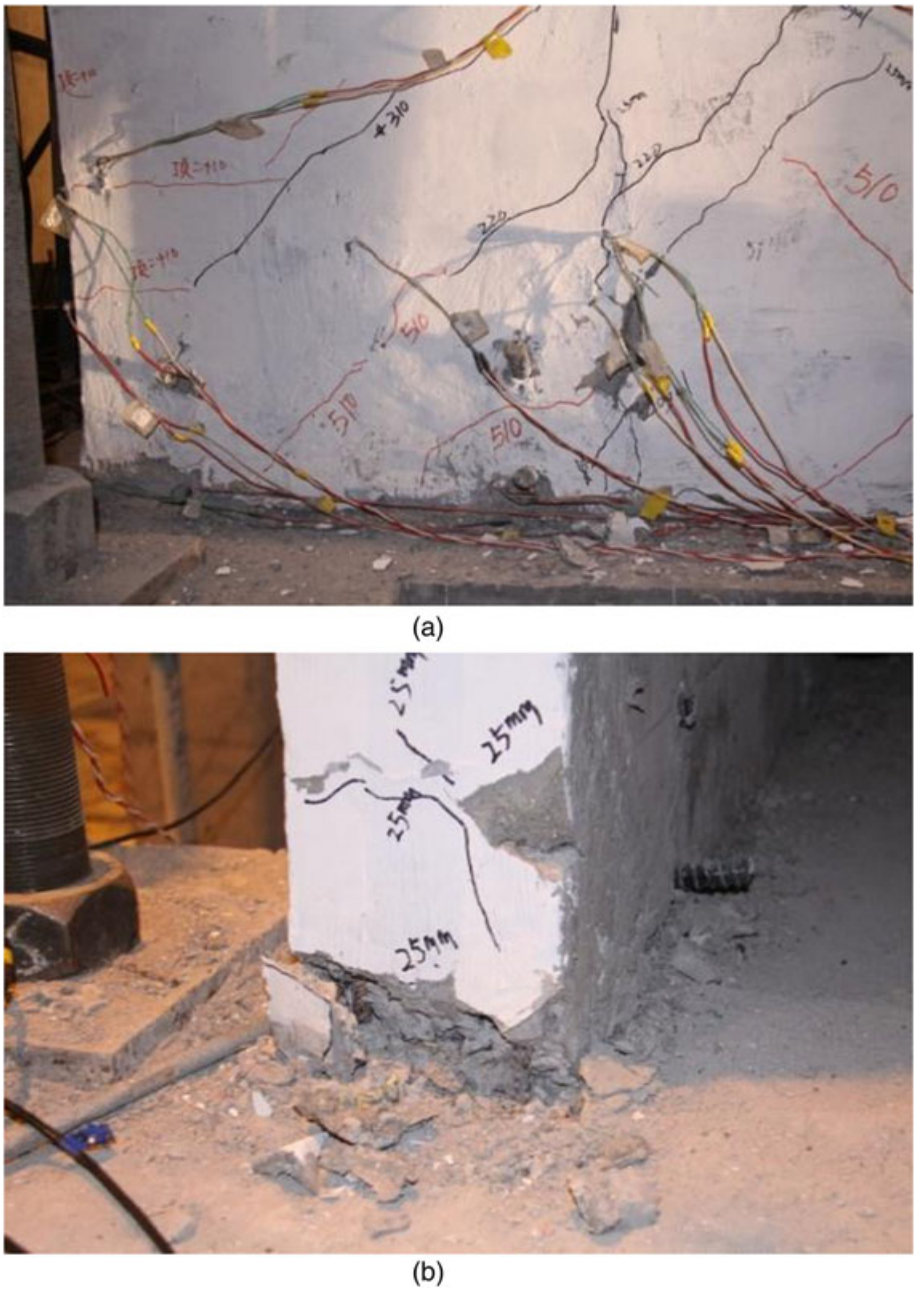

FIGURE 21 Failure mode of the wall limb on first story for 620 gal peak ground acceleration: (a) R5 on Line D; (b) right corner of R4 on Line D

5.1.2 | Failure modes of the coupling beam

There was no damage to the coupling beam for PDSTs with PGAs of 70 and 125 gal, and the corresponding maximum interstory drift was 0.68 mm. The first series of inclined cracks of the coupling beam on Line F occurred at the boundary of the shear wall and coupling beam, as shown in Figure 16 for a PDST with a PGA of 220 gal, and the corresponding maximum interstory drift was 8.9 mm. The cracks started from the edge of the opening extent inclined to the shear wall. For a PDST with a PGA of 400 gal, the corresponding maximum interstory drift was 17.6 mm, the previous cracks constantly widened, and cross cracks were visible, as shown in Figure 17. The damage of the coupling beam was repairable. For a PDST with a PGA of 620 gal, the corresponding maximum interstory drift was 27.5 mm and the cross cracks increased, accompanied by the spalling of the concrete and the baring of the horizontal steel bars on the top corner region of the openings, as shown in Figure 18.

5.1.3 | Failure modes of the wall limb

There were no visible cracks on the wall limbs for PDSTs with PGAs of 70 and 125 gal, and the corresponding maximum interstory drift was 0.68 mm. For PDSTs with a PGA of 220 gal, the corresponding maximum interstory drift was 8.9 mm and the first series of horizontal cracks on the wall limb occurred at the bottom of the first story, as shown in Figure 19.

When subjected to a PGA of 400 gal, the corresponding maximum interstory drift was 17.6 mm, the previous cracks constantly expanded and inclined in their extension, as shown in Figure 20. More horizontal and inclined cracks were visible, especially at the middle region of

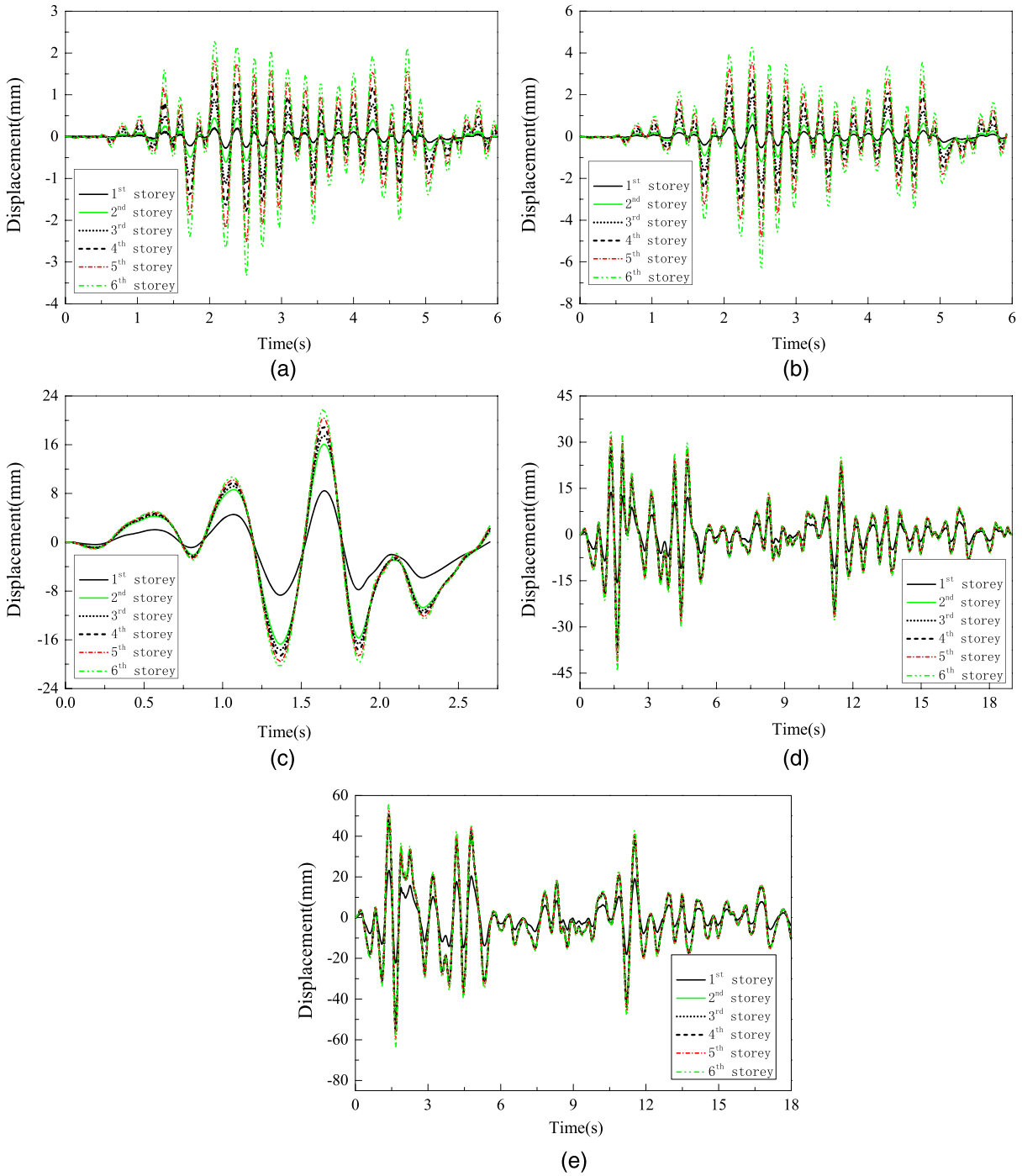

FIGURE 22 Displacement responses to the El Centro earthquake record: (a) histories for 70 gal peak ground acceleration (PGA); (b) histories for 125 gal PGA; (c) histories for 220 gal PGA; (d) histories for 400 gal PGA; (e) histories for 620 gal PGA

Line F. The cement mortar crashed at the right corner of R4 on Line D. The damage to the wall limb appeared to be repairable.

When subjected to a PGA of 620 gal, the corresponding maximum interstory drift was 27.5 mm and the cross cracks widened, accompanied by the crashing and displacement of concrete at the bottom corner region on the first story, as shown in Figure 21. More inclined cracks were visible, especially in the middle region of Line F.

5.2 | Displacement responses

The displacement responses of the structure subjected to PDSTs are presented in Figure 22. The displacement responses of the first and second stories are the average of the two measured deformations of the specimen in each story, such as the average of d11 and d12, for the first story or the average of d21 and d22 for the second story. The first modal response of the structure was activated by earthquake waves. It is shown from Figure 22 that the displacement response histories for 125 gal PGA are nearly linear related to the displacement response histories for 70 gal PGA. This means the structure exhibited elastic behavior and suffered limited damage when subjected to these earthquakes. The conclusion is consistent with the test observations in Subsection 5.1 that there was no visible damage on the infilled walls, coupling beams, and wall limbs when the structure was subjected to PGAs of 70 and 125 gal. The displacement time histories for higher

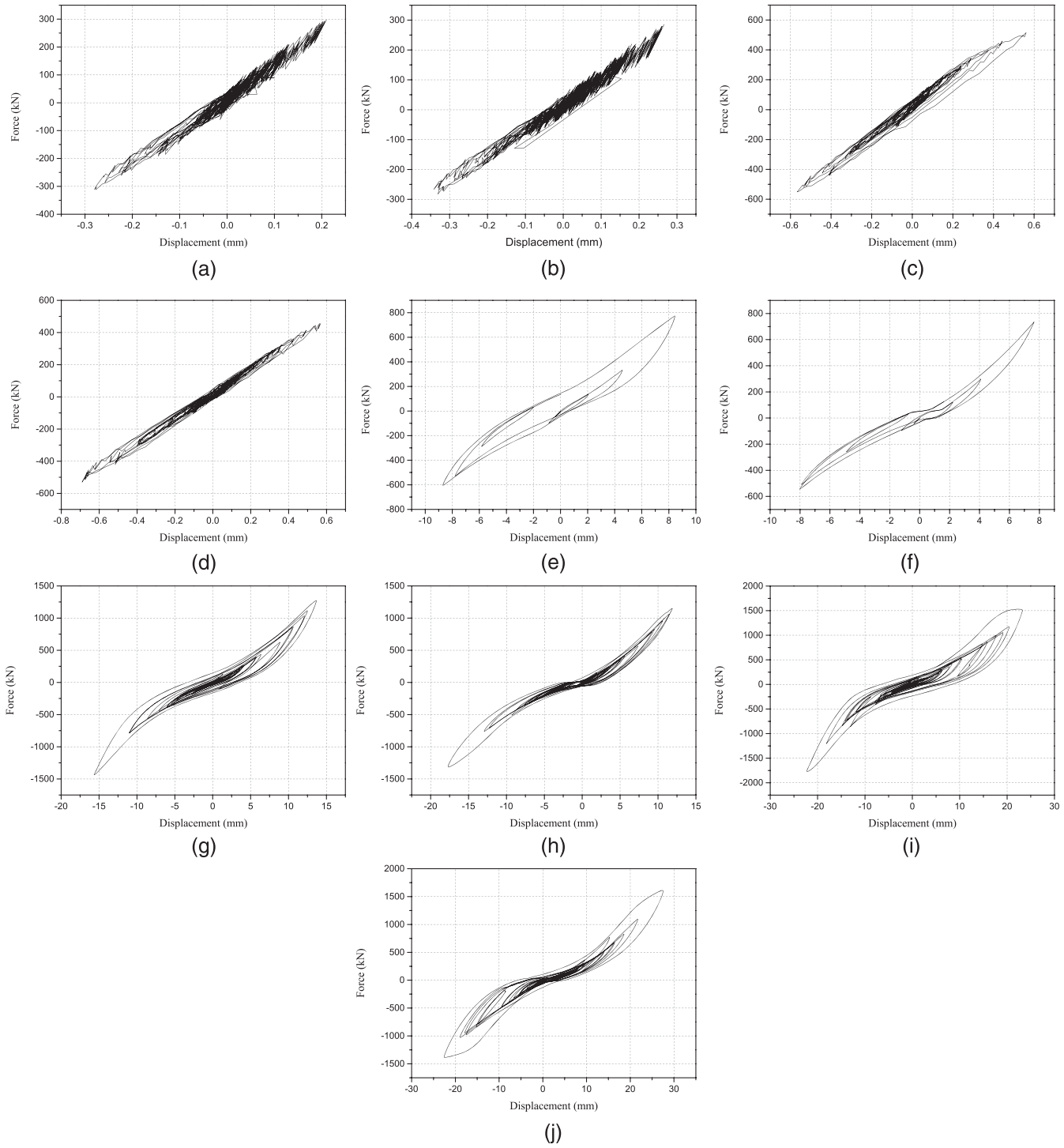

FIGURE 23 Force-displacement hysteretic responses of the specimen from pseudodynamic substructure testings: (a) first story response for 70 gal peak ground acceleration (PGA); (b) second story response for 70 gal PGA; (c) first story response for 125 gal PGA; (d) second story response for 125 gal PGA; (e) first story response for 220 gal PGA; (f) second story response for 220 gal PGA; (g) first story response for 400 gal PGA; (h) second story response for 400 PGA; (i) first story response for 620 gal PGA; (j) second story response for 620 gal PGA

TABLE 6 Maximum interstory drift angle from PDSTs

	70 gal		125 gal		220 gal		400 gal		620 gal	
Story	+	−	+	−	+	−	+	−	+	−
1	1/14493	1/11538	1/5347	1/5300	1/365	1/337	1/219	1/193	1/129	1/134
2	1/13453	1/9118	1/5272	1/4437	1/392	1/375	1/297	1/170	1/109	1/133

Note. PDST = pseudodynamic substructure testing.

level intensity of earthquakes were obviously different, and this means that the specimen suffers higher levels of damage with the increase of the PGA. The conclusion is also consistent with the test observations in Subsection 5.1 that there were different levels of damage on the infilled walls, coupling beams, and wall limbs when the structure was subjected to PGAs of 220, 400, and 620 gal.

5.3 | Force-displacement responses

Force-displacement curves of the specimen from PDSTs are presented in Figure 23. It can be deduced that for lower values of PGA (70 and 125 gal) the forces in the first and second stories were linearly related to the displacement responses. This means the structure suffered limited the damage when subjected to these earthquakes. The conclusion is consistent with the test observations in Subsection 5.1 that there was no visible damage on the infilled walls, coupling beams, and wall limbs when the structure was subjected to PGAs of 70 and 125 gal. Hysteretic loops were traced also for PDSTs with PGAs of 220, 400, and 620 gal. The areas of the hysteretic loops clearly increased with the PGA increase. This indicates that the specimen suffered from different levels of damage on the infilled walls, coupling beams, and wall limbs, and the energy dissipation increased with the PGA increase. The conclusion is also consistent with the test observations in Subsection 5.1 that different levels of damage were present on the infilled walls, coupling beam, and wall limb, when the structure was subjected to PGAs of 220, 400, and 625 gal.

5.4 | Interstory drift angles

The interstory drift angle, which is defined as the relative deformations between two consecutive floors divided by the interstory height in this paper, is analyzed also to disclose the seismic performance of the investigated structure. The maximum interstory drift angles of the specimen from PDSTs are shown in Table 6. It is shown that the maximum interstory drift angle corresponding to 70 gal was 1/9118, which is less than the limitation of the elastic interstory drift angle of 1/1000. Likewise, the maximum interstory drift angle associated to 400 gal was 1/170, which is less than the limitation of the elastic–plastic interstory drift angle of 1/120; and the maximum interstory drift angle corresponding to 620 gal was 1/109, while the structure did not collapse or exhibited severe damage. As a result, the PDST results indicate that the investigated six-story PBSRCSWs structure exhibited a favorable seismic behavior.

6 | CONCLUSIONS

The building configuration and the corresponding wall-to-wall and wall-to-floor connections for a PBSRCSWs were conceived and analyzed in this paper. Then, the PDST platform HyTest combined with EDFC (HyTest with EDFC) was presented and experimentally validated. Successively, the responses of the proposed connections and the seismic performance of the six-story PBSRCSWs were experimentally studied by means of full-scale PDSTs. The main conclusions of this research work are summarized herein.

1. The box module, chosen as the basic assembling element in PBSRCSWs, provides high-quality and easy assembly production with minimal construction time. As a result, the method appears to have wide potential applications for civil engineering structures.
2. Three types of connection were proposed and applied together for the PBSRCSWs: (a) a horizontal wall-to-wall connection characterized by vertical reinforcements spliced indirectly by single-row grout-filled sleeves; (b) a vertical wall-to-wall connection characterized by a stirrup bolted with vertical reinforcements; (c) a horizontal non-composite wall-to-floor slab connection. The relevant joints exhibited good performances in terms of configuration and easy assembly.
3. The high-accuracy PDST platform, that is, the HyTest with EDFC, was proposed and experimentally validated. Experimental results showed that the HyTest endowed with the EDFC method can realize accurate control on structural deformations and provide high-accuracy experimental results, especially for PDSTs with relatively small PGAs. As a result, the HyTest with EDFC appears to have wide application prospects for seismic testing of civil engineering components or structures.
4. The damages of the structure exhibited during different levels of earthquake wave record were concentrated on the infilled walls, coupling beams, and wall limbs; no visible damage occurred on the proposed horizontal and vertical wall-to-wall connections and wall-to-floor slab connections. The PDST results indicate that the proposed connections perform well for the investigated six-story PBSRCSWs.
5. The PBSRCSWs exhibited excellent seismic performance in PDSTs. In particular, subjected to El Centro (NS, 1940) earthquake wave record, the maximum interstory drift angle of the specimen was 1/9118 with a PGA of 70 gal and 1/170 with a PGA of 400 gal. The specimen did not exhibit severe damage or collapse even at 620 gal PGA.

ACKNOWLEDGEMENTS

The National Key Research and Development Program of China (Grant 2016YFC0701106), the National Science Foundation of China (Grants 51161120360, 51308159, and 51408157), and A Set of Technology Study and Engineering Application Examples for Building Industrialization in Yunnan Province (2012CA025) are acknowledged by the authors for supporting the study of this paper. The authors also thank Mr. Yunfei Ma for his effort to coordinate the laboratory activities.

REFERENCES

[1] M. Safdie, *PCI. J.* **1967**, *12*(1), 60.

[2] M. J. N. Priestley, *PCI J.* **1991**, *36*(4), 50.

[3] E. Henin, G. Morcous, *Eng. Struct.* **2015**, *83*, 154, DOI: 10.1016/j.engstruct.2014.10.045.

[4] S. M. Kang, O. J. Kim, H. G. Park, *Eng. Struct.* **2013**, *56*, 1645, DOI: 10.1016/j.engstruct.2013.07.036.

[5] J. Sun, H. Qiu, Y. Lu, *Struct. Des. Tall Special Build*. Published online in Wiley Online Library **2016**, DOI: 10.1002/tal.1277.

[6] B. Erkmen, A. E. Schultz, *J. Earthq. Eng.* **2009**, *13*(7), 1047, DOI: 10.1080/13632460902859136.

[7] F. J. Perez, R. Sause, S. Pessiki, *J. Struct. Eng. ASCE* **2007**, *133*(11), 1531, DOI: 10.1061/(ASCE)0733-9445(2007)133:11(1531).

[8] B. J. Smith, Y. C. Kurama, M. J. McGinnis, *J. Struct. Eng. ASCE* **2011**, *137*(10), 1052, DOI: 10.1061/(ASCE)ST.1943-541X.0000327.

[9] B. J. Smith, Y. C. Kurama, M. J. McGinnis, *J. Struct. Eng. ASCE* **2013**, *139*(11), 1917, DOI: 10.1061/(ASCE)ST.1943-541X.0000755.

[10] J. I. Restrepo, A. Rahman, *J. Struct. Eng. ASCE* **2007**, *133*(11), 1560, DOI: 10.1061/(ASCE)0733-9445(2007)133:11(1560).

[11] S. Sritharan, S. Aaleti, R. S. Henry, K. Y. Liu, K. C. Tsai, *Earthq. Eng. Struct. Dyn.* **2015**, *44*(12), 2075, DOI: 10.1002/eqe.2576.

[12] O. S. Bursi, G. Gramola, *Mater. Struct.* **2000**, *33*(3), 154, DOI: 10.1007/BF02479409.

[13] P. A. Bonnet, M. S. Williams, A. Blakeborough, *Earthq. Eng. Struct. Dyn.* **2008**, *37*(13), 1467, DOI: 10.1002/eqe.821.

[14] O. S. Bursi, A. Gonzalez-Buelga, L. Vulcan, S. A. Neild, D. J. Wagg, *Earthq. Eng. Struct. Dyn.* **2008**, *37*(3), 339, DOI: 10.1002/eqe.757.

[15] S. Y. Chang, *J. Eng. Mech.,ASCE* **2007**, *133*(7), 748, DOI: 10.1061/(ASCE)0733-9399(2007)133:7(748).

[16] C. Chen, J. M. Ricles, T. M. Marullo, O. Mercan, *Earthq. Eng. Struct. Dyn.* **2009**, *38*(1), 23, DOI: 10.1002/eqe.838.

[17] Z. X. Chen, G. S. Xu, B. Wu, Y. T. Sun, H. D. Wang, F. L. Wang, *Earthq. Eng. Struct. Dyn.* **2014**, *43*(7), 969, DOI: 10.1002/eqe.2382.

[18] C. P. Lamarche, A. Bonelli, O. S. Bursi, *Earthq. Eng. Struct. Dyn.* **2009**, *38*(9), 1071, DOI: 10.1002/eqe.884.

[19] B. Wu, Q. Wang, P. B. Shing, J. P. Ou, *Earthq. Eng. Struct. Dyn.* **2007**, *36*(9), 1127, DOI: 10.1002/eqe.674.

[20] B. Wu, G. S. Xu, Q. Y. Wang, M. S. Williams, *Earthq. Eng. Struct. Dyn.* **2006**, *35*(3), 293, DOI: 10.1002/eqe.519.

[21] Z. Wang, B. Wu, O. S. Bursi, G. S. Xu, Y. Ding, *Smart Struct. Syst.* **2014**, *14*(6), 1247, DOI: 10.12989/.2014.14.6.1247.

[22] Y. Chae, J. M. Ricles, R. Sause. **2014**. Real-time hybrid simulation with specimen feedback data. *The Sixth World Conference on Structural Control and Monitoring–6WCSCM*, Barcelona (Spain), July 15-17, No. 49.

[23] B. Dong, R. Sause, J. M. Ricles, *Earthq. Eng. Struct. Dyn.* **2015**, *44*(12), 2035, DOI: 10.1002/eqe.2572.

[24] G. Ou, A. I. Ozdagli, S. J. Dyke, B. Wu, *Earthq. Eng. Struct. Dyn.* **2015**, *44*(3), 441, DOI: 10.1002/eqe.2479.

[25] T. Wang, N. Yoshitake, P. Pan, T. H. Lee, M. Nakashima, *Earthq. Eng. Struct. Dyn.* **2008**, *37*(2), 265, DOI: 10.1002/eqe.755.

[26] O. S. Kwon, V. Kammula, *Earthq. Eng. Struct. Dyn.* **2013**, *42*(13), 1971, DOI: 10.1002/eqe.2307.

[27] B. Wu, T. Wang, *Smart Struct. Syst.* **2014**, *14*(6), 1105, DOI: 10.12989/sss.2014.14.6,1105.

[28] G. Abbiati, O. S. Bursi, P. Caperan, L. Di Samo, F. J. Molina, F. Paolacci, P. Pegon, *Earthq. Eng. Struct. Dyn.* **2015**, *44*(13), 2221, DOI: 10.1002/eqe.2580.

[29] Y. Takahashi, G. L. Fenves, *Earthq. Eng. Struct. Dyn.* **2005**, *35*(3), 267, DOI: 10.1002/eqe.518.

[30] O. S. Kwon, N. Nakata, A. Elnashai, B. Spencer, *J. Earthq. Eng.* **2005**, *9*(5), 741, DOI: 10.1142/S1363246905002158.

AUTHOR BIOGRAPHIES

Guoshan Xu is an associate professor of Civil Engineering in Harbin Institute of Technology, Harbin, China. He achieved his PhD from Harbin Institute of Technology in 2010, worked as a visiting PhD student at University of California, San Diego, in 2008, and worked as a visiting scholar at University of Trento, Italy, in 2011. His research interests lie in precast shear wall structures and structural seismic testing technology.

Zhen Wang is an assistant professor of Civil Engineering in Harbin Institute of Technology, Harbin, China. He achieved his PhD from Harbin Institute of Technology in 2012, worked as a visiting PhD student at University of Trento, Italy, in 2010. His research interests lie in structural seismic testing technology.

Bin Wu is a professor of Civil Engineering in Harbin Institute of Technology, Harbin, China. He achieved his PhD from Harbin Institute of Technology in 1998, worked as a visiting scholar at Oxford University in 2002 and University of California, San Diego, in 2006. His research interests lie in precast shear wall structures, structural passive and semi-active control of buildings, and structural seismic testing technology.

Oreste S. Bursi graduated in Mechanical Engineering at the University of Padua in 1984 and achieved his PhD in Mechanical Engineering at the University of Bristol. He is a full professor of Structural Dynamics and Control at the University of Trento. The research activity is mainly devoted to the pseudodynamic test method, nonlinear dynamics, control, and structural identification. http://r.unitn.it/en/dicam/nhmsdc, http://me.unitn.it/oreste-bursi/

Xiaojing Tan is an engineer of Yunnan Institute of Building Research, Kunming, China. He achieved his PhD from Harbin Institute of Technology in 2013. His research interests lie in precast shear wall structures and structural seismic testing technology.

Qingbo Yang is an engineer of Jiangsu Power Design Institute Co., Ltd. of China Energy Engineering Group, Nanjing, China. She achieved her master's degree from Harbin Institute of Technology in 2015. Her research interests lie in precast shear wall structures.

Long Wen is pursuing master's degree in Harbin Institute of Technology, Harbin, China. His research interests lie in precast shear wall structures.

Hongbin Jiang is an associate professor of Civil Engineering in Harbin Institute of Technology, Harbin, China. His research interests lie in precast shear wall structures and masonry structures.

How to cite this article: Xu G, Wang Z, Wu B, et al. Pseudodynamic tests with substructuring of a full-scale precast box-modularized structure made of reinforced concrete shear walls. *Struct Design Tall Spec Build*. 2017;26:e1354. https://doi.org/10.1002/tal.1354